COMPUTER-AIDED DESIGN & APPLICATIONS, 2018
VOL. 15, NO. 3, 318–329
https://doi.org/10.1080/16864360.2017.1397883

Printability analysis in additive manufacturing

Radu I. Corcodel and Horea T. Ilies

University of Connecticut, USA

ABSTRACT

In recent years Additive Manufacturing (AM) has advanced from design and fitting validation to biomedical, rapid tooling, tissue engineering, the arts and even food manufacturing. The corresponding scale reduction did not coincide with improving two of the most important process characteristics, namely print accuracy and build time. In this paper we introduce a computational framework for computing the maximum build volume for given non-circular extruders and printing machines that have 2, 3 and perhaps higher number of degrees of freedom (DOF). The proposed method also outputs the accessible configuration space of a multi-DOF AM machine that is instrumental in planning the final (temporal) motion of single or multiple print heads. Furthermore, we show that the proposed method allows the ranking of multiple extruders based on their volumetric deviation from nominal geometry. This formulation makes no assumption about the number of machine DOFs, nor about the planarity of the target contour, making it applicable to emerging AM technologies such as 6-axis printing with non-planar layers, and layer-less additive manufacturing.

KEYWORDS

Additive manufacturing; accuracy; inverse motion; multi-parameter motions; non-planar layers; layer-less additive manufacturing

1. Introduction

An important issue in Additive Manufacturing (AM), which to this date is still not well addressed, is predicting the build accuracy and its relationship to the total build time. For example, in Fusion Deposition Modeling (FDM), the accuracy of the as-manufactured geometry can be partially controlled in-process by choosing a convenient in-fill pattern [14] or modulating the printing head speed and nozzle temperature around small area features. Though, the effects of this process optimization are ultimately limited by the kinematic configuration of the AM machine as well as by the geometry and size of the extruder. On the other hand, the latter two factors have the greatest potential for improving the build accuracy and, in particular, without negatively impacting the build time. Furthermore, more general machine kinematics offering the ability to print on non-planar surfaces, particularly in conjunction with non-circular print heads, could reduce not only the print time required by the model itself, but also decrease the amount and complexity of the required support structure with all its implications on the ultimate cost of the 3D printing.

The nozzle's shape has been traditionally yet, perhaps, unnecessarily constrained to be circular, and the printing of small features imposes an upper bound on the size of the nozzle. However, the smallest printable feature, or print resolution [4], is fundamentally limited by both the shape and dimensions of this extruder along with the usual material-related parameters [1]. This resolution can be improved locally in-process by controlling the filament flow rate or under/over extrusion [19], although the extruder geometry remains a significant contributing factor to the build accuracy.

Fig. 1 presents a conceptual example of a small U-shaped feature which must be printed as close to nominal geometry as possible. Fig. 1(a) shows a smaller circular extruder and the simplest trajectory of its center that would maintain the extruder within the given contour. It is clear that the print head must execute at least seven linear interpolations to fill this contour, while the elliptical extruder of Fig. 1(b) can execute just three. The asymmetry of the elliptical extruder with respect to its center also allows it to navigate in the narrower regions of the contour, for example the bottom passage. Such an asymmetry can prove to be very useful also in the case of printing machines which have rotational kinematic axes, such as Selective Compliance Assembly Robot Arms (SCARA) [9], Delta and Hexa architectures [10],[20]. In the case of Hexa machines or other *6*-axis configurations [8], a non-circular extruder can exploit more efficiently the motion of the print head, resulting in an improved precision and a faster build time. For this simple case, the choice is clear, but for more complex outlines and *non-planar* layers it is unclear what might be the "optimal" shape of

CONTACT Radu I. Corcodel, radu.corcodel@uconn.edu; Horea T. Ilies horea.ilies@uconn.edu

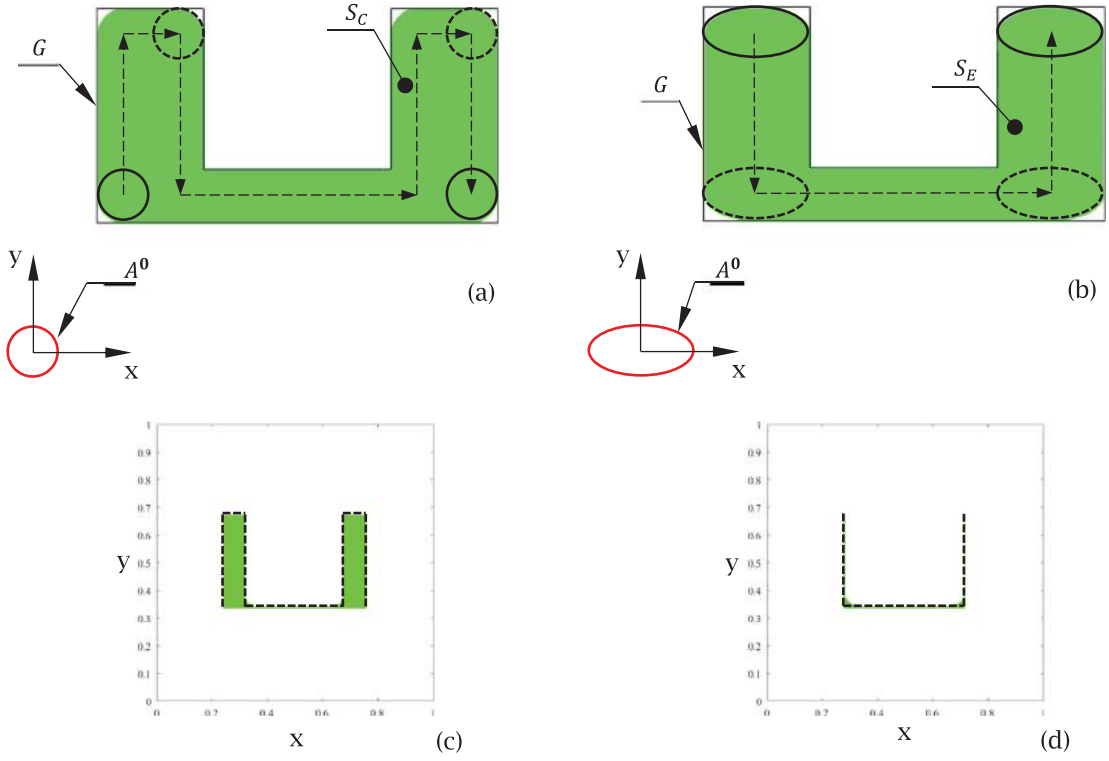

Figure 1. Solid fill of a target contour with extruders of different profiles: (a) circular, (b) elliptical. Figures (a) and (b) show the simplest motion of the nozzle without exceeding the limit of the contour. The corresponding set of configurations where the nozzles are contained inside the contour are shaded in green in Figures (c) and (d). Any time-based motion M is a coupling of the parameters x and y, and it is a curve in the parametric space (here shown dotted) defined by these configurations.

the extruder. In fact, there seems to be no published literature addressing this important aspect of 3D printing. Perhaps the most up-to-date published information can be found in a recent paper examining the properties of as-manufactured parts for layered AM with standard print heads [16].

In this paper we present a generic method relying on the properties of the inverted trajectory [11],[12] to identify the subset of the machine configurations for which a hot-end nozzle of known but arbitrary geometry is guaranteed not to exceed the 3D boundary of a given model. Our formulation makes no assumptions about the planarity of the target contour (i.e., possibly a non-planar slice of a 3D boundary), nor about the machine's number of Degrees of Freedom (DOF) generically denoted here by p; hence our formulation can be effectively used in all emerging Additive Manufacturing processes, such as 6-axis FDM printing. By examining the intersection set between the nozzle geometry and the inverse trajectory of points sampled from the target volume we determine the total set of motion parameters for which the nozzle is permanently contained within the target contour. This allows us to compute the maximum built volume as a sweep, defined by the nozzle's "smallest printable feature" [4],[16] and the restricted p-parameter motion (assuming a constant extrusion flow and constant velocity of the printing head). This, in turn, provides a ranking of given nozzle geometries in terms of their corresponding build accuracy and subsequently build time. We can then compute the volumetric deviation between the built and the nominal volume, as a Lebesgue measure defined over the set difference between the two respective volumes. Given this restriction, the problem of motion synthesis, which is the problem of coupling the DOF of the machine to one independent parameter such as time, recasts in our framework as the problem of finding a space filling curve [3], under certain build quality requirements, such as surface roughness [2]. The motion synthesis topic is outside the scope of this paper and will be covered in a subsequent publication.

2. Conceptual example - inverse trajectory

In general, the trajectory T_x of a point is defined as

$$T_x = \bigcup_{s \in M} x^s \tag{2.1}$$

where $s \in SE(3)$ are configurations of a family of rigid-body motions M, generated by arbitrary kinematic linkages, such as a robotic arm. Although in this paper we

focus on rigid motions, our formulation is generic and extends to affine transformations. A configuration s of a system, such as a robot arm, is defined by a set of p generalized coordinates (e.g., joint angles, prismatic translations, etc.), that are fundamentally independent. This allows us to parametrize the motion M, by a vector space of parameters $u \in R^p$, where $u = [u_1, u_2 \dots u_p]^t$ is a column vector containing the mechanism's generalized coordinates. Therefore each configuration $s \in M$ is identified by at least one vector u, and denoted with $s(u)$. In this paper we adopt a similar notation system as in [15]. A general mapping ($SE(3)$ toE^3) that considers all generalized coordinates to be independent, rather than dependent variables, is in general non-physical and referred to as multi-parametric motion [5]. The physical motion of such a system can be obtained by coupling the generalized parameters by one single parameter, often *time*, which is the task of motion planning [15], and results in a *one*-parameter variety. As an example, the Euclidean workspace of a representative point of a 5-axis CNC machine is in general a 3D volume containing *all* possible spatial locations of that point that can be achieved by that particular machine (with uncoupled parameters). At the same time, the trajectory of the same point under a (coupled) one-parameter motion is usually a curve, which is a subset of the machine's workspace.

In other words, the trajectory of a point moving according to a p-parameter motion in E^d is a p-dimensional set if $p \leq d$, or a d-dimensional entity if $p > d$. It is worth noting that the multi-parameter trajectory of a point is the superset of all one-parameter trajectories that can possibly be synthesized in a time-based reference system. By applying the inverse transforms $r \in SE(3)$ such that $r(u) \oplus s(u) = \mathrm{id}_d$ to a sample point $y \in E^d$, where id_d is the d-dimensional Identity transformation, we obtain the so-called inverse trajectory of the sample point y, similarly defined as

$$\hat{T}_y = \bigcup_{r \in \hat{M}} y^r \tag{2.2}$$

In this formulation, $\oplus$ is the group additive operator, and $\hat{M}$ is the set of inverse transformations, also known as the inverted motion (see also [11]); for example, if the transformations are represented as homogeneous transformation matrices, then the group operator is the usual multiplication of matrices, and the inverse transformations are given by matrix inverse. The property of the inverse trajectory states that only the points $x \in \hat{T}_y$ will pass through the sample point y during the motion M [7],[12], which can be readily verified from the definition of the inverse transformation $r = \hat{s}$. Importantly, this property applies without restrictions to the number of motion parameters and the dimensionality of the Euclidean space where the points are embedded since it has a generic set theoretical formulation.

To provide a visual aid, Fig. 2 shows in solid color the one-parameter inverse trajectory $\hat{T}_y$ of an arbitrary point y, embedded in a two-dimensional Euclidean plane. Point y is contained in the forward trajectories of all points $x \in \hat{T}_y$, but not contained in the forward trajectory of any point $z \notin \hat{T}_y$. This property has an important application in workspace analysis because it allows one to determine exact the subset $X \subseteq A$ of a moving set $A \subset E^d$ (such as the end-effector of a robot arm) which will "visit" a workspace location $y \in E^d$ during some arbitrary motion M. Namely, the subset X is determined from the set intersection $X = A^{s(\mathbf{0})} \cap \hat{T}_y$, where $A^{s(\mathbf{0})}$ is the configuration of the moving set A positioned at the initial parameter values $u_0 \equiv \mathbf{0} = [0, 0 \dots 0]^t$. In the notation $\mathbf{0} = [0, 0 \dots 0]^t$ we implied a normalized parametric range $u \in [\mathbf{0}, \mathbf{1}]$, although this is not a requirement of our formulation, but merely a way of denoting the initial

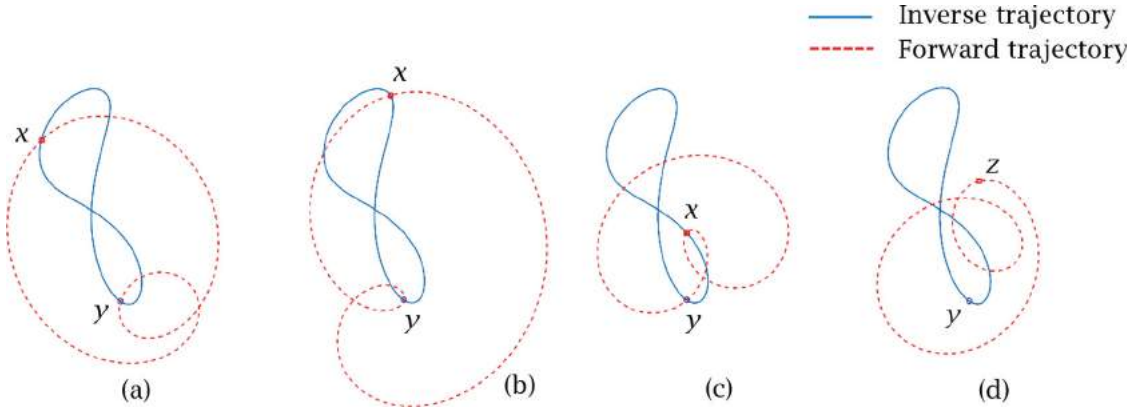

Figure 2. The inverse trajectory of a random point $y \in E^2$ shown here in solid blue color. Fig. 2(a) through 2(c): the forward trajectory of any point $x \in \hat{T}_y$ intersects point y. Fig. 2(d): in the Euclidean space there are no points $z \notin \hat{T}_y$ which will pass through y during the forward motion.

motion configuration. Also for brevity, we denote $A^{s(\mathbf{0})}$ simply with A^0, and refer to it as the "initial configuration" of the moving set A. Furthermore, via a set intersection, we can determine all parameter values u at which the set A sweeps the target point y. This is achieved by using a Point Membership Classification (PMC) function $I : R^p \times E^d \to \{0, 1\}$, defined as

$$I(u, y) = \begin{cases} 1, \text{ if } A^0 \cap y^{r(u)} \neq \emptyset \\ 0, \text{ otherwise} \end{cases} \tag{2.3}$$

This indicator function $I(u, y)$ will be used in Section 3 to determine a restriction on the motion parameter space R^p for which the opening of a 3D printing nozzle can only move inside a given geometry of arbitrary complexity.

3. Formulation

As stated in the Introduction section, in this paper we seek to derive a computational framework to determine the maximum volume that can be built using a known extruder of arbitrary design, without exceeding the boundary of a given a nominal geometry. Ideally the built geometry should be identical to the target geometry (i.e. no over- or under-fill of the target contour). A factor that significantly limits the build accuracy is the shape and size of the print nozzle, since its resolving power degrades rapidly around small features such as sharp corners and bosses. The repeatability and precision of the mechanical structure is also an important factor that influences the geometric and dimensional tolerance of the built part, but since this topic is beyond the scope of this paper, we shall consider the ideal case when the positioning tolerance of the machine is negligible.

The maximum volumetric deviation between the as-manufactured and the nominal geometry can be formulated in terms of Maximum Material Condition (*MMC*) tolerance. More information about geometric tolerances such as MMC, least material condition (*LMC*) and the reciprocity condition can be found in ISO 2692 and ISO/TC 213. In addition, we can provide a ranking of several given extruders in terms of the deviation of the corresponding as-manufactured geometries from the nominal geometry. The highest ranking extruder will have the smallest MMC tolerance, or, in other words, the largest volume of deposited material without exceeding the target boundary of the nominal geometry. The key to our formulation is to compute a restriction of the printing head's motion, represented as a set of configurations, for which the nozzle is fully contained in the target domain. We represent all motion configurations as points in a p–dimensional space where p is the number of generalized coordinates, as described in Section 2. Thus a restriction of the motion is nothing else than a set $\mathcal{P} \subset R^p$. To prevent any confusion, we denote sets of the usual Euclidean space with uppercase letters (i.e. A, X, G, etc.) and sets of the parametric space with a stylized font (i.e. $\mathcal{B}$, $\mathcal{C}$, $\mathcal{P}$ etc.).

In our case, if $y \in G$ is a point of the target geometry $G \subset E^d$, and $A^0 \subset E^d$ is the nozzle geometry in its initial configuration, the parameter vectors u for which the inverse trajectory $\hat{T}_y$ intersects the nozzle geometry A^0 are precisely the motion parameters at which the nozzle A passes through point y of the target G during the given (forward) motion. The indicator function I, introduced in Section 2, allows us to accumulate a set of configurations $\mathcal{C} \subset R^p$, where $\mathcal{C} = \{u \in R^p : I(u, y) = 1, \forall y \in G\}$. In other words, the parametric range $\mathcal{C}$ contains all motion parameter values where the nozzle can potentially deposit material over the target G. The complete set $\mathcal{C}$ also contains the parameters for which the extruder deposits material both inside and outside of the target geometry. This is unwanted since we want to enforce an MMC tolerance. These undesirable motion parameters, which are elements of a subset $\mathcal{B} \subset R^p$ and defined by $\mathcal{B} = \{u \in R^p : I(u, x) = 1, \forall x \in \partial G\}$, are those parametric values for which the extruder intersects the boundary of the target geometry. The parametric set which will enforce the MMC tolerance is given by $\mathcal{P} = \mathcal{C} \setminus \mathcal{B}$.

To illustrate, Fig. 3 shows a simplified example where the extruder A can only move on a single horizontal axis between two extreme configurations. The shape of the extruder is circular, and the nominal geometry G is a rectangle aligned with the motion direction. For illustrative purposes we assume that the height of the contour is identical to the diameter of the nozzle, so that the contour can be filled with a single pass along the axis of motion. By accumulating all parameter values at which the inverse trajectories of samples $y_i \in G$ intersect the nozzle in its initial configuration, we effectively determine *all* extruder configurations where material can be deposited over G, including those for which the nozzle extrudes both inside and outside the boundary of G. If the rapid prototyping machine extrudes within the configuration range $\mathcal{B}$, the nozzle *only* extrudes over the boundary of the target geometry. Consequently, when the machine extrudes in the range $\mathcal{P} = \mathcal{C} \setminus \mathcal{B}$, the built geometry is guaranteed to be not over-extruded because set $\mathcal{P}$ contains only those parameter values for which the nozzle in fully contained in set G, and thus enforcing the maximum material condition.

Even though in all our examples we assume that process parameters (material flow, print-head speed, etc.) that determine the shape and size of the smallest printable feature [16] remain constant during motion, this is not

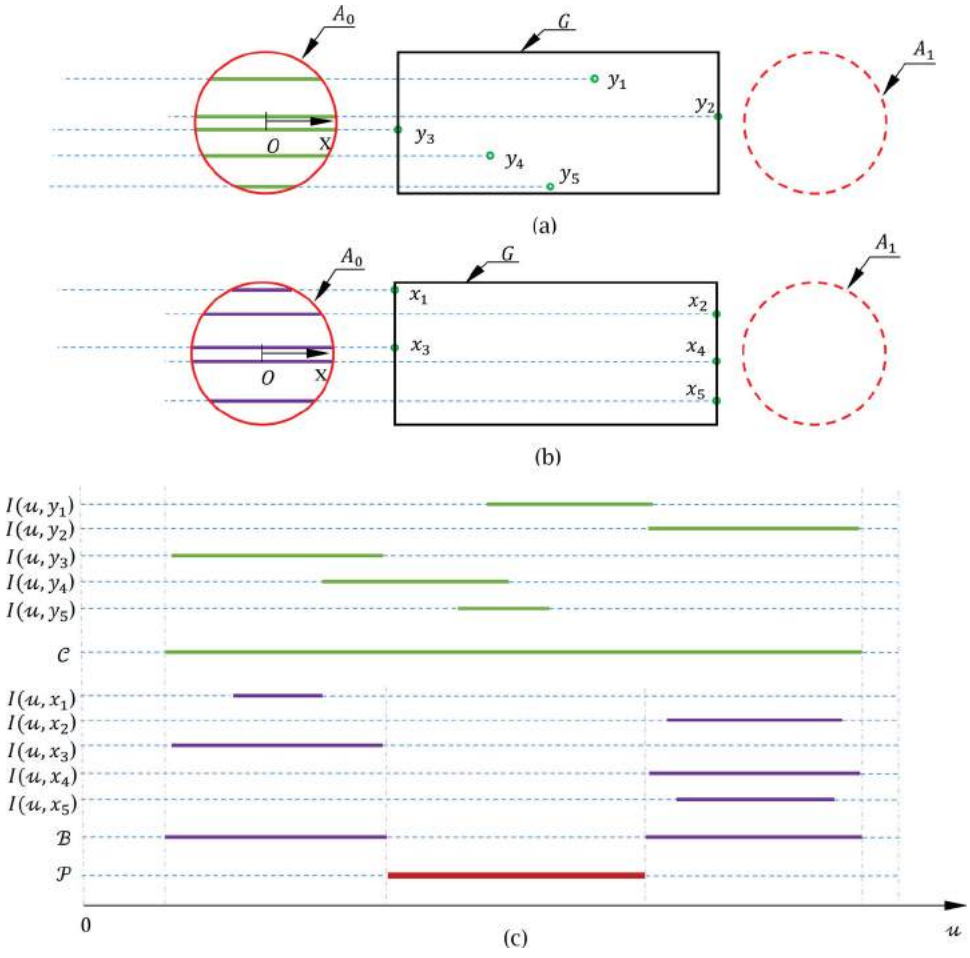

Figure 3. Determining the motion parametric range of a circular extruder A, enforcing the MMC tolerance. Fig. (a) and (b) show the inverse trajectories of sample points $y_i \in G$ and $x_i \in \partial G$, and their respective intersection set with the circular nozzle A^0 in its initial configuration. In Fig. (c), the subset $\mathcal{C}$ subsumes all motion parameters where the nozzle geometry sweeps over the target contour, while the subset $\mathcal{B}$ contains only the parameters where the extruder sweeps the boundary ∂G. The set $\mathcal{P} = \mathcal{C} \setminus \mathcal{B}$ is the set of parameters for which the nozzle is completely contained within the target contour.

a limiting factor. In fact, the formulation proposed here remains valid and can be applied to even more general cases involving deformations of the deposited material as long as they can be incorporated as additional variables, or non-rigid motions, in the motion parametrization [6].

The restriction $\mathcal{P}$ allows us to determine the build volume (see Fig. 4) corresponding to the MMC tolerance as a solid sweep. We determine this using the usual definition of a sweep [7], where the transformations applied to the nozzle's geometry A are parametrized by vectors of the subset $\mathcal{P}$.

$$S_{MMC} = \bigcup_{u \in \mathcal{P}} A^{s(u)} \tag{3.1}$$

In this formulation we can also perform an automatic selection of nozzle geometry based on the volumetric deviation between the maximum built geometry S_{MMC} relative to the nominal geometry G. More specifically, the highest ranking nozzle will correspond to the smallest Lebesgue measure of the set difference $\min[\lambda(G \backslash S_{MMC_i})]$, where i represents the i-th hot-end nozzle we are comparing. In Section 5 we present a brief discussion showing that critical regions of the build volume such as sharp corners and thin bosses, which would otherwise be missed by the extruder, can be included in the nozzle's path by relaxing locally the parametric restriction $\mathcal{P}$.

Figures 5 and 6 provide simple examples using our formulation. In Fig. 5 the nozzle can translate in the XY plane. The elliptical nozzle in Figure 5(b) not only has a larger built volume (S_2) than the built volume due to the circular extruder, but can also resolve the sharp corners with a higher accuracy. For illustration, the figure also shows the volume S_1 swept by the nozzle A in the parametric restriction $\mathcal{B}$. The built volume in Fig. 5(b) is also larger because the nominal geometry is conveniently aligned with the semi-major axis of the asymmetric extruder. This shows that a Cartesian Rapid

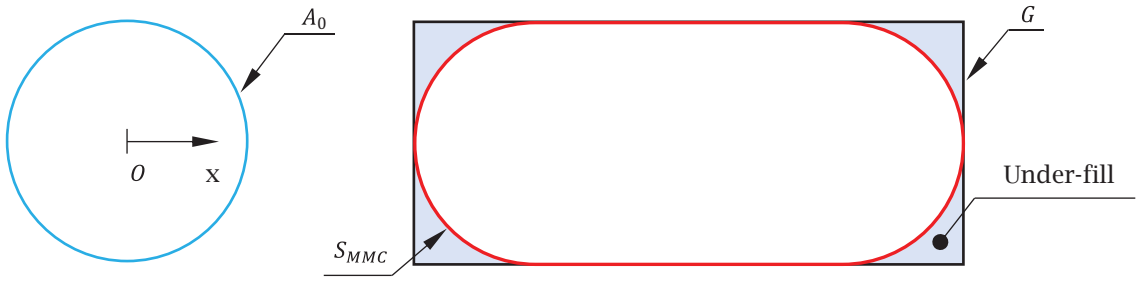

Figure 4. Sweep of nozzle *A* from Fig. 5 in the parameter range $\mathcal{P}$. The figure shows the under-fill areas created by enforcing the MMC tolerance condition.

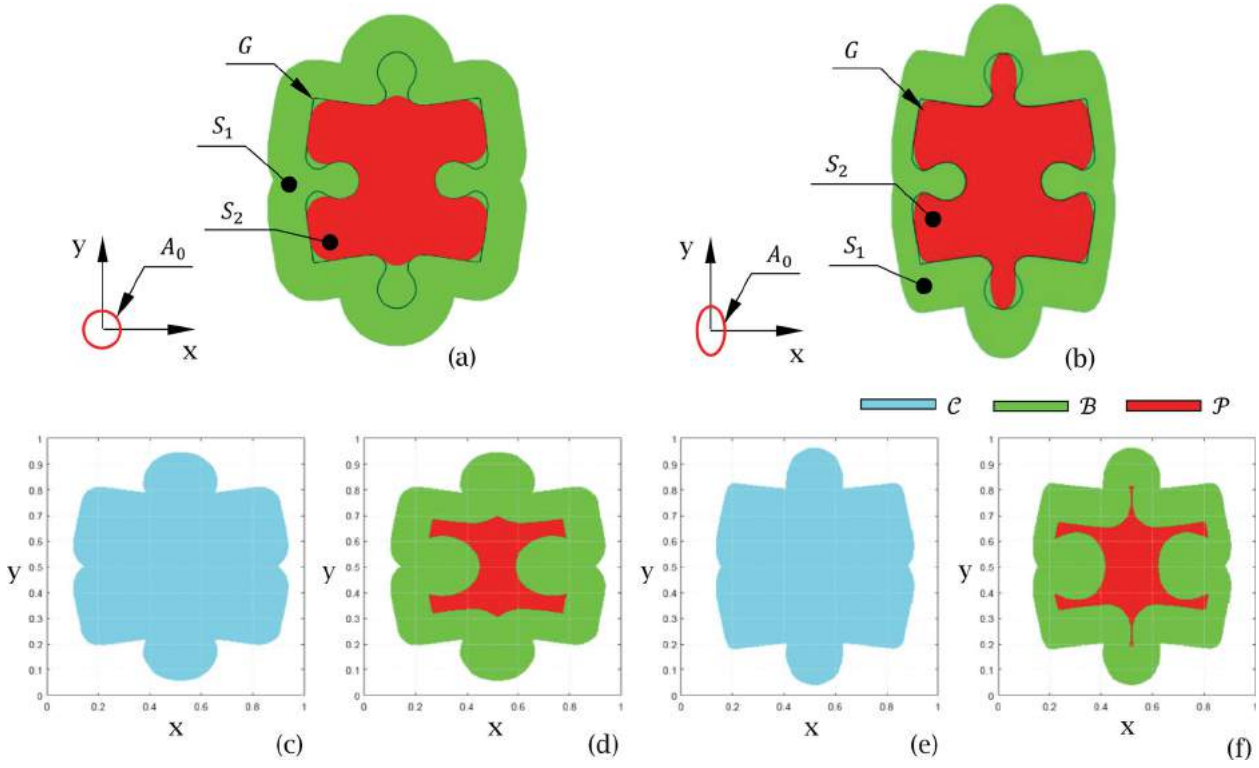

Figure 5. Side-by-side comparison of two extruders: Fig. (a) circular, Fig. (b) elliptical. The AM machine is a classic *2.5*-axis Cartesian structure. Fig. (c) and (d) show the parametric domain corresponding to the circular extruder of Fig. (a). Fig. (e) and (f) correspond to the elliptical extruder in Fig. (b).

Prototyping machine cannot fully take advantage of the asymmetric shape of an extruder unless the target contour is intentionally placed along one of the principal directions of the extruder. On the other hand, a machine that allows print-head rotations can reorient the nozzle so that, regardless of geometry orientation, the extruder can be brought in a convenient orientation which provides maximum local precision. Section 4.2 presents a comparative example using a Cartesian and a T-T-R machine fitted with elliptical extruders, in which the built volume generated by the Cartesian machine and elliptical nozzle has a smaller accuracy than the volume generated with a circular extruder.

In Fig. 6 the available motions are one rotation about the nozzle's axis and one translation. In this case an asymmetric extruder can take advantage of the extra rotation and navigate through narrow passages. The set theoretic formulation implies that our method allows both translations and rotations, unlike other approaches based on mathematical morphology [17]. A further advantage of our method is its invariance to the dimensionality of the parametric space. In principle, any arbitrary motion with as many degrees of freedom is supported. Moreover there are no restrictions on the planarity of the build contour, thus paving the road forward for applications in multi-axis FDM printing and other emerging Additive

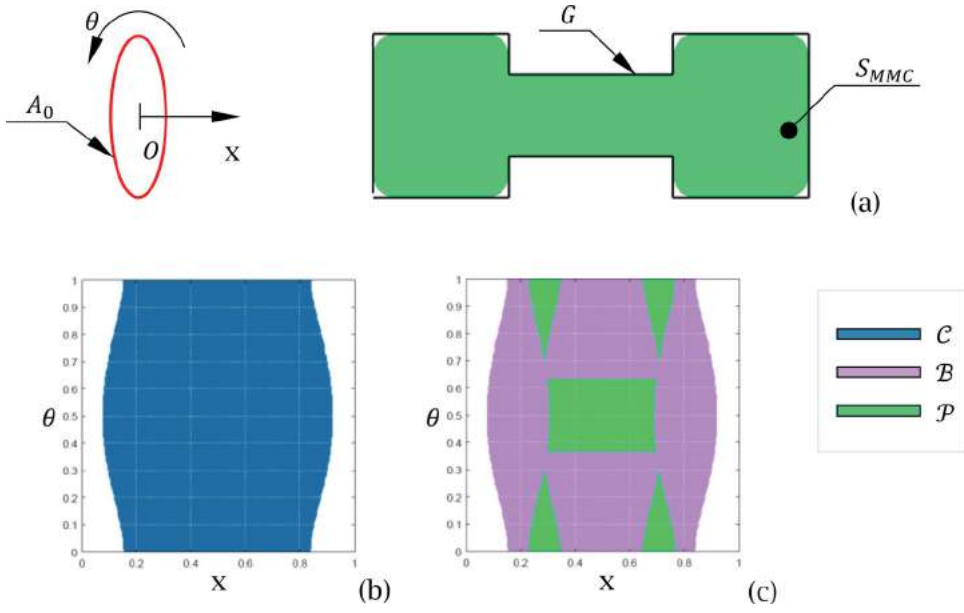

Figure 6. (a): Elliptical extruder attached to a 2DOF structure (Rotation and Translation). The elliptical extruder can navigate through the narrow passage despite having a large major radius compared to the dimensions of the contour. Fig. (b) shows the parameter selection corresponding to the set $\mathcal{C}$, while Fig. (c) shows the selection $\mathcal{B}$ and $\mathcal{P}$ as described earlier.

Manufacturing processes. We present an example of such a case in the next section.

4. 2D/3D Layered and layer-less examples

4.1. Single layer build

In this test case, we show a comparison in build accuracy between two machines which have attached a circular and an elliptical extruder nozzle. Fig. 7 shows a circular extruder capable of a planar *XY* motion. The "keep-in" contour is a sketch of Japan's coastline. To emphasize the deviation between the nominal and built geometry, we chose an extruder large in comparison to the small features of the target contour *G*. As expected, the build area deviates significantly from the nominal geometry, simply because the extruder is too large to extrude over the small features without over-filling. The example additionally shows that our method is completely impervious to disconnected sets. In this case, there have been identified

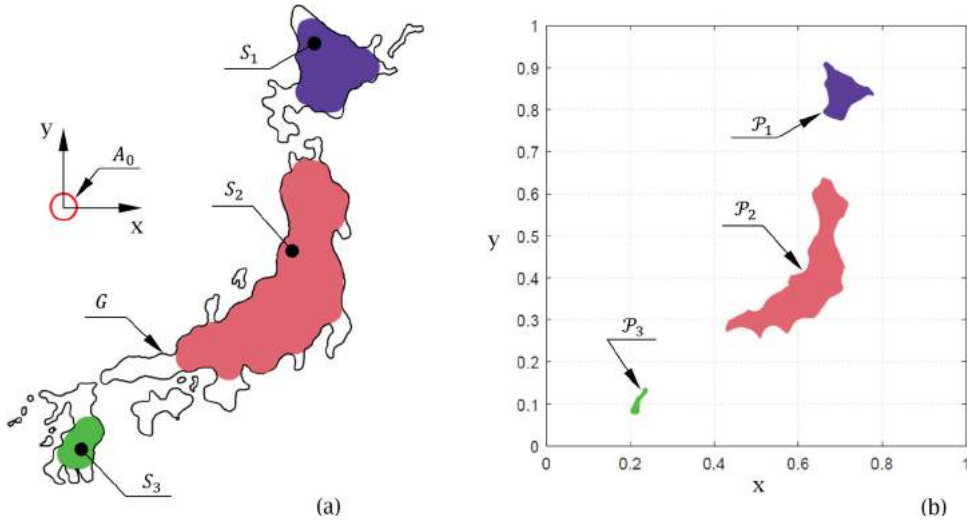

Figure 7. Circular nozzle A^0 in a planar *XY* motion. The target contour contains many small features that will otherwise be difficult to print using an oversized extruder. Fig. (b) shows the parameter selections $\mathcal{P}_i$ which will ensure the nozzle stays inside the contour at all times. This examples shows that our formulation is inherently capable of processing arbitrary *n*-dimensional geometry, while at the same time is able to detect disconnected sets of the parameter domain which must be printed individually.

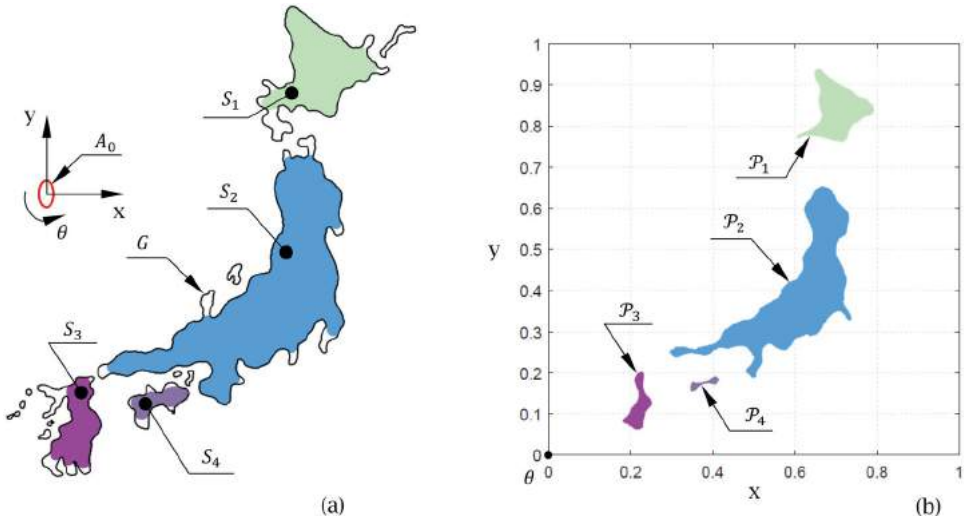

Figure 8. Elliptical nozzle A^0 attached to a T-T-R machine. The extra degree of freedom (the rotation about the extruder's axis) permits the asymmetric extruder to cover more of the nominal geometry without exceeding the target boundary. In addition, this configuration is capable of printing a fourth region S_4 of the nominal geometry. The increase in build surface area is 17.62% as compared to the combined build areas of the circular extruder shown in Fig. 7.

three different sets which must be printed sequentially or, depending on equipment, simultaneously using multi-extruder print heads. Here $S_i = \text{sweep}[A, M(\mathcal{P}_i)]$ represents the sweep of nozzle A under the parametric selection $\mathcal{P}_i$, and is mathematically given by $S_i = \cup A^{s(u)}$, where $u \in \mathcal{P}_i$.

Fig. 8 shows a more complicated example where an elliptical extruder is attached to the printing head of a T-T-R machine. The possible motions allowed by the mechanical structure are the rotation about the extruder's axis and two planar translations. The shape of the asymmetric extruder in Fig. 8 is exploited by the extra rotation and allows for a better coverage of the nominal set. In fact the build area of the elliptical extruder is 17.62% greater than it was in Fig. 7, thus ensuring a better coverage of the nominal geometry.

4.2. Volumetric build with planar layers

The application in Fig. 9 depicts a 3D geometric model built with a circular and respectively, an elliptical extruder. In this example the nominal model from Fig. 9(a) is sliced in 278 layers, using a commercial mesh processing software. This allows us to reiterate our computation over the total number of layers. Fig. 9(b) shows the built geometry using a circular extruder and a classical Cartesian machine. To emphasize the printability of small features we scaled down the model to dimensions comparable to the nozzle size. The circular extruder in this example acts as a low-pass filter, smoothing the model texture loosing most of the small features. In Fig. 9(c) the same Cartesian machine is used in combination with an elliptical extruder. Since there are no rotations, the machine cannot take advantage of the nozzle asymmetry resulting in a built model that has a "preferred" direction, aligned with the semi-major axis, where small feature are better resolved. To emphasize this effect, we oriented the nozzle so this direction is aligned with the x-axis (left to right in the image). Because of this less than optimum orientation, the built model shows a poorer resolution when compared to the one in Fig. 9(b). Finally, in Fig. 9(d) the model is built using the same elliptical extruder but this time on a T-T-R machine configuration. The extra rotation about the extruder's center axis allows the nozzle to cover small features in any planar direction, and thus following more closely the nominal geometry. Using this configuration, we achieved a 4.2% increase in build volume, compared to the model in Fig. 9(c).

Fig. 9 (e) through (f) show a section of the computed volumetric builds. In Fig. 9(e), corresponding to the model in Fig. 9(b), the extruder used is circular and is capable of translating in the XY plane. It is clear that small features of the layer contour (shown in black) cannot be printed because the size of the extruder is too large. Fig. 9(f) corresponds to the model (c) and shows the use of an elliptical extruder in planar translation. The asymmetry of the extruder and the lack of rotation favors the x-axis in terms of precision. In this machine setup, a printable feature G_2 that is aligned with the x-axis can be printed with much higher accuracy than the feature G_1, which is aligned with the y-axis. Lastly, in Fig. 9(g) the elliptical extruder has an extra rotation about its center axis. This ensures that the minor radius of the nozzle can

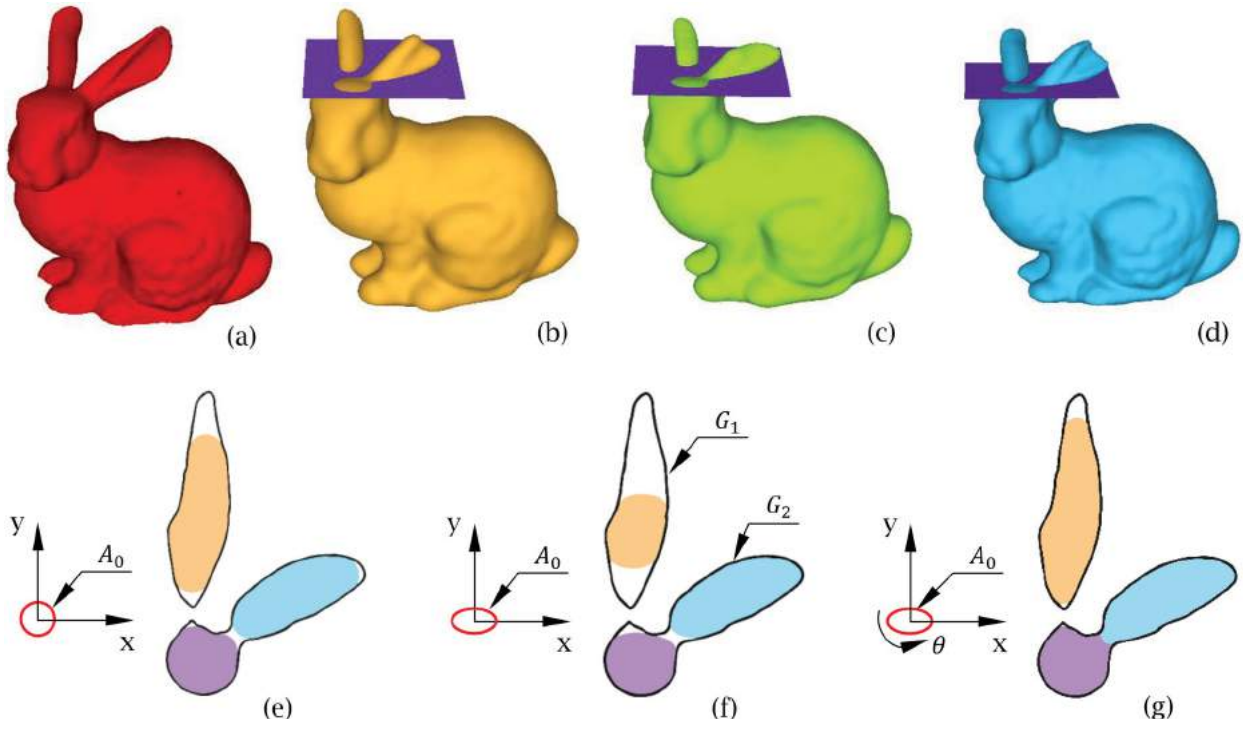

Figure 9. Computed 3D build. Fig. (a) shows the nominal geometry to be printed; here the planar layers are aligned with the Z-axis. Fig. (b): the model is built using a circular print head on a Cartesian 3D printer. Fig. (c) shows a build using a Cartesian machine but an elliptical extruder. Since the mechanical structure does not allow rotations, the nozzle's asymmetry produces two fixed directions of different resolving power. Fig. (d) illustrates a model where a T-T-R mechanism is used in conjunction with an elliptical extruder. Due to the extra rotation about the nozzle's axis, the printer can resolve finer detail than both Fig. (b) and (c) while maintaining a similar material flow and thus a comparable build time. Fig. (e) through (g) illustrate a cross-section from the respective models (b), (c) and (d), and the volume of material deposited in that layer. The figures also show the shape and size of the extruders used (A^0).

be used in any orientation and thus resolving smaller features, regardless of their orientation with respect to the build volume. Out of the three machine configurations under study, the model in Fig. 9(d) has the largest build volume, without exceeding the boundary of the nominal geometry, thus the best MMC tolerance.

Our GPU accelerated algorithm is a straight-forward implementation of the method described in Section 3, and uses point clouds and homogeneous transformation matrices to carry out the computation. The machine used to run this software is a Dell Precision 7910 with dual Xeon processor clocked at 2×2.3GHz, an nVidia Quadro K2200 graphics card and 64GB of RAM. Using this configuration we achieve on average an execution time of approximately 37s for each of the models in Fig. 9.

4.3. 3D "layer-less" build: an example for medical application

In this example we show how this method can be applied to "layer-less" 3D printing of shapes as a cost-effective and accurate alternative to 3D build volumes, printed with Selective Laser Sintering (SLS) [13],[18]. In this example the printing is achieved using a 4-DOF Selective Compliance Assembly Robot Arm (SCARA), shown in Fig. 10. The mechanical structure of this robot has 4 DOF that include a displacement of the nozzle along the z-axis, as well as three rotations about the local z-axes. Importantly, the method presented in the paper can be applied to printing with devices that have multiple degrees of freedom and print on planar as well as non-planar surfaces.

Naturally, the medical destination of these builds requires the deposited material to be USP-NF class VI compliant and meet the ISO-10993 standard for biocompatible thermoplastics. In this application we use FDM, without the need of depositing the material in a classic layer-by-layer approach. In our formulation, the motion of the printing head is not restricted to a plane. Therefore we can compute the part's geometry without a pre-set build direction or constant thickness layers. As described in the Formulation section, we identify all print-head configurations for which the extruder nozzle is contained within the 3D boundary of the nominal geometry, and compute the maximum built geometry as a sweep defined by the extruder's smallest printable feature transformed by a restricted set of configurations. Once this information is available, one can explore the motion planning

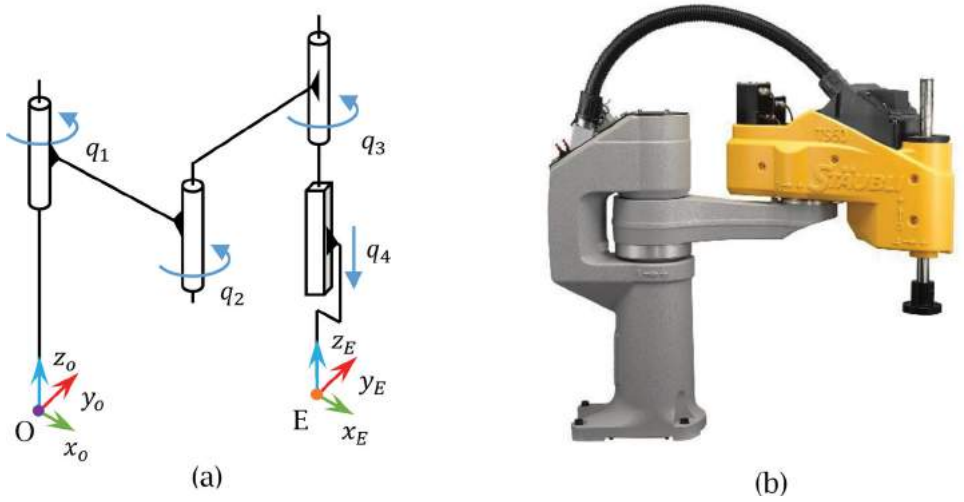

Figure 10. Selective Compliance Assembly Robot Arm (SCARA). Fig. (a) shows the kinematic configuration. The Origin reference system (O) is fixed in the 3D space while the End-effector system (E) has 4-DOF relative to O (i.e. R-R-R-T). Fig. (b) shows a commercial version of this machine, produced by Stäubli.

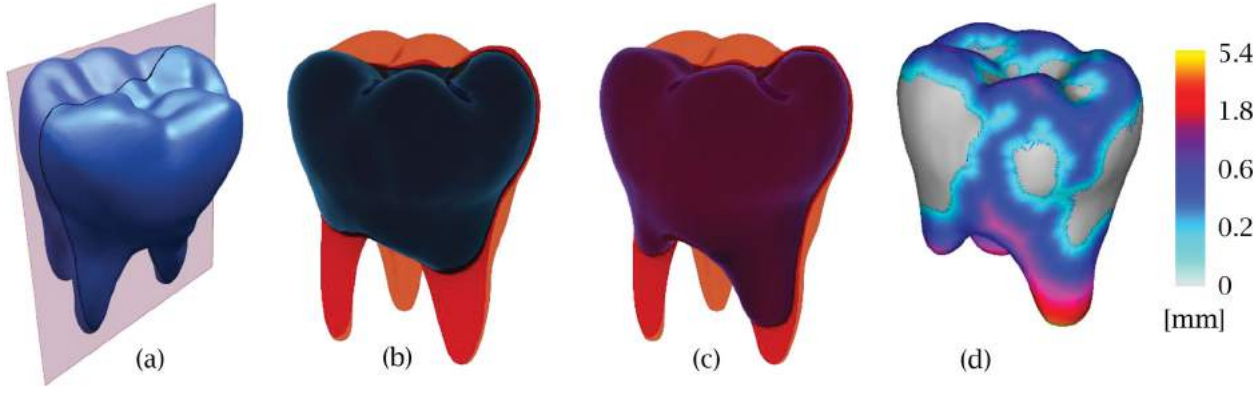

Figure 11. Conceptual dental implant built with oversize extruders. Fig. (a) shows the nominal geometry of the "implant". The maximum built geometries are shown in: Fig (b) using a circular extruder with an opening of $\phi 2.15mm$, Fig. (c) using an elliptical extruder with semi-axes $a = 1.28mm$ and $b = 2.15mm$. Fig. (d) shows the additional volume added by the elliptical extruder, when compared to the as-built geometry generated by the circular extruder.

aspects of this "layer-less" 3D printing, which we will discuss in a subsequent paper.

The nominal geometry in this example is an average-sized maxillary first molar of an adult. To emphasize the difference in built volume, we first present the maximum built geometry using oversized extruders with a circular, and respectively an elliptical opening. Fig. 11(a) shows the nominal geometry of the molar as well as the position of the section plane used in the corresponding section views. Fig. 11(b) and (c) show how the oversized extruders cannot resolve the small features corresponding to the roots of the molar. In Fig. 11(d) we color code the thickness of the additional volume of material deposited by the elliptical extruder compared to the circular one. The figure shows that only the low curvature sections of the model can be printed with the same accuracy by the two extruders.

In Fig. 12 we show a more realistic 3D build of this first molar. The circular extruder of $\phi 1.28mm$, which is regarded as a relatively large nozzle, does not adequately print the roots of the molar, making it unsuitable for this application. On the other hand an elliptical extruder of the same semi-major axis but a semi-minor axis of $a = 0.71mm$ achieves a higher geometric accuracy, while maintaining the benefits of using a relatively large nozzle, including decreased printing time and increased durability. Even though the difference between the as-built and nominal volumes shown here is below 5%, the method that we present here can identify the small features of the nominal model that cannot be printed with given nozzle geometries and machine kinematics. For a side-by-side comparison, Figure 12(b) shows a cross-section of the 3D models using the course extruders.

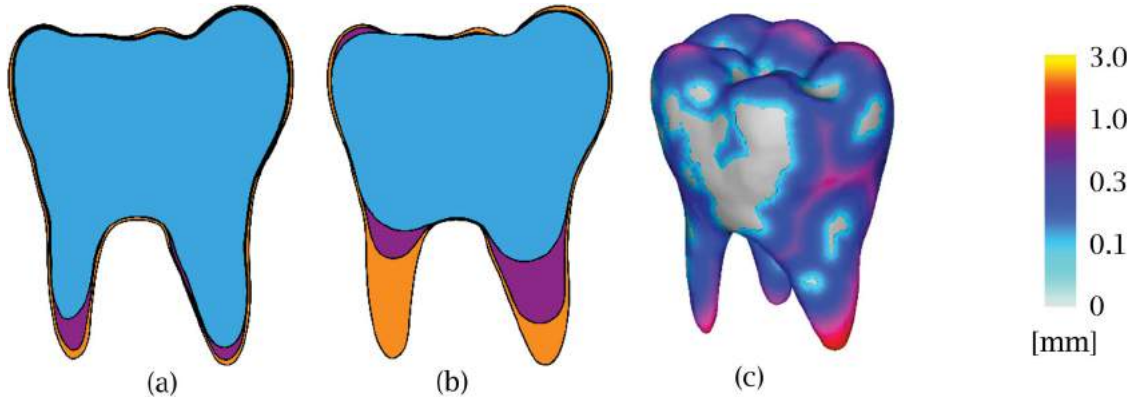

Figure 12. Superimposed maximum built geometries of a first molar using a $\phi 1.28mm$ circular extruder (in blue) and an elliptical extruder with semi-axes $a = 0.71mm$ and $b = 1.28mm$ (in purple). Fig. (b) shows a cross-section of the 3D models from Fig. 11 for a comparison of accuracy. Fig. 12(d) illustrates the additional volume deposited by the elliptical extruder compared to the geometry of the as-built geometry generated the circular extruder.

5. Conclusions

In this paper we present a generic method for computing the maximum build geometry in additive manufacturing, which, in turn, provides a ranking of given nozzle geometries in terms of their corresponding build accuracy and subsequently build time. It is important to note that this method is applicable to printing on planar and non-planar surfaces, with extruders of arbitrary geometry and with machine kinematics that have multiple degrees of freedom, including rotations. We enforce the Maximum Material Condition as a dimensional tolerance to have a meaningful comparison of build volumes. In effect, this tolerance acts as a maximizer of the built volume while ensuring that the nominal boundary is not exceeded. We exemplify the effectiveness of our method with an elliptical extruder as an alternative to nozzles with a circular opening, although our generic method accepts any arbitrary geometry.

Our formulation is derived in set theoretical terms and uses the concept of the inverse trajectory, which allows it to be implemented in virtually any geometric representation which supports distance computations. We do not consider time in our derivations; instead we treat the motion as a set of configurations parametrized by the mechanism's generalized coordinates. The ability to calculate the motion restriction which will prevent the nozzle from exceeding the nominal boundary can be viewed as a precursor to motion synthesis. Any one-parameter coupling of all generalized coordinated is represented in this parametric space as a curve. Therefore, a re-parametrization of this motion under time (i.e. motion planning) recasts itself as a space spanning curve in a p-dimensional space, given certain quality requirements. This formulation does not enforce the planarity of the build layer, which makes our approach suitable for layer-less AM technologies such as 6-axis Fusion Deposition Modelling and laser jet cladding.

The mathematical framework presented here provides all the information necessary for a subsequent as-manufactured geometry optimization. By relaxing locally the MMC condition, the build accuracy can be further improved locally by over-extrusion. Such an analysis can be carried in the parameter domain, for example by mapping the over-extruded geometry as a signed distance function from the boundary. Such an approach would identify and correct boundary regions where the built accuracy exceeds a target value.

The proposed method opens up a number of fascinating research directions to explore, which would take advantage of the additional flexibility of noncircular print heads driven by multi-DOF machines along non-planar surfaces.

Acknowledgements

This work was supported in part by the National Science Foundation grants CMMI-1462759, IIS-1526249, and CMMI-1635103.

ORCID

Radu I. Corcodel http://orcid.org/0000-0003-2867-6451

References

[1] Ahn, S. H.; Montero, M.; Odell, D.; Roundy, S.; Wright, P. K.: Anisotropic material properties of fused deposition modeling ABS, *Rapid prototyping journal*, 8(4), 2002, 248–257. https://doi.org/10.1108/13552540210441166

[2] Ahn, D.; Kweon, J. H.; Kwon, S.; Song, J.; Lee, S.: Representation of surface roughness in fused deposition modeling, *Journal of Materials Processing Technology*, 209(15), 2009, 5593–5600. https://doi.org/10.1016/j.jmatprotec.2009.05.016

[3] Asano, T.; Ranjan, D.; Ross, T.; Welzl, E.; Windmayer, P.: Space filling curves and their use in the design of geometric data structures, *Latin American Symposium on Theoretical Informatics*, 181, 1997, 36–48. https://doi.org/10.1016/s0304-3975(96)00259-9

[4] Au, A. K.; Lee, W.; Folch, A.: Mail-order microfluidics: evaluation of stereolitography for the production of microfluidic devices, *Lab on a Chip*, 14(7), 2014, 1294–1301. https://doi.org/10.1039/C3LC51360B

[5] Bothema, R.; Roth, B.: *Theoretical kinematics*, Dover Publication, New York, 1990.

[6] Erdim, H.; Ilies, H. T.: A comparison of sampling strategies for computing general sweeps, *Computer-Aided Design*, 42(8), 2010, 657–669. https://doi.org/10.1016/j.cad.2009.06.002

[7] Erdim, H.; Ilies, H. T.: Classifying points for sweeping solids, *Computer-Aided Design*, 2008, 40(9), 987–998. https://doi.org/10.1016/j.cad.2008.07.005

[8] Gazeau, J. P.; Said, Z.; Ramirez-Torres, G.: A novel 5-axis robot for printing high resolution pictures from media on 3D wide surfaces, Industrial Technology, IEEE International Conference, ICIT 2009, 1–6. https://doi.org/10.1109/icit.2009.4939735

[9] Hamade, R. F.; Zeineddine, F.; Akle, B.; Smaili, A.: Modelangelo: a subtractive 5-axis robotic arm for rapid prototyping, *Robotics and Computer-Integrated Manufacturing*, 21(2), 2005, 133–144. https://doi.org/10.1016/j.rcim.2004.06.004

[10] Hesselbach, J.; Bier, C.; Campos, A.; Lowe, H.: Direct kinematic singularity detection of a hexa parallel robot, Robotics and Automation, *Proceedings of the 2005 IEEE International Conference*, 2005, 3238–3243. https://doi.org/10.1109/robot.2005.1570609

[11] Ilies, H. T.; Shapiro, V.: The dual of sweep, *Computer-Aided Design*, 31(3), 1999, 185–201. https://doi.org/10.1016/S0010-4485(99)00015-9

[12] Ilies, H. T.; Shapiro, V.: On shaping with motion, *Journal of Mechanical Design, ASME transactions*, 122(4), 2000, 567–574. https://doi.org/10.1115/1.1319319

[13] Jardini, A. L.; Larosa, M. A.; Maciel Filho, R.; de Carvalho Zavaglia, C.A.; Bernardes, L. F.; Lambert, C. S.; Calderoni, D. R.; Kharmandayan, P.: Cranial reconstruction: 3D biomodel and custom-built implant created using additive manufacturing, *Journal of Cranio-Maxillofacial Surgery*, 42(8), 2014, 1877–1884. https://doi.org/10.1016/j.jcms.2014.07.006

[14] Kruth, J. P.; Leu, M. C.; Nakagawa, T.: Progress in additive manufacturing and rapid prototyping, *CIRP Annals-Manufacturing Technology*, 47(2), 1998, 525–540. https://doi.org/10.1016/S0007-8506(07)63240-5

[15] Latombe, J. C.: *Robot motion planning*, Springer Science & Business Media, Vol. 124, 2012.

[16] Nelaturi, S.; Shapiro, V.: Representation and analysis of additively manufactured parts, *Computer-Aided Design*, 2015, 13–23. https://doi.org/10.1016/j.cad.2015.03.007

[17] Serra, J.; Soille, P.: Mathematical morphology and its applications to image processing, Springer Science and Business Media, Vol. 2, 2012

[18] Sing, S. L.; An, J.; Yeong, W. Y.; Wiria, F. E.: Laser and electron-beam powder-bed additive manufacturing of metallic implants: A review on processes, materials and designs, *Journal of Orthopaedic Research*, 34(3), 2016, 369–385. https://doi.org/10.1002/jor.23075

[19] Turner, B. N.; Strong, R.; Gold, S. A.: A review of melt extrusion additive manufacturing processes: I. Process design and modelling, *Rapid Prototyping Journal*, 2014, 192–204. https://doi.org/10.1108/RPJ-01-2013-0012

[20] Vischer, P.; Clavel, R.: Kinematic calibration of the parallel Delta robot, *Robotica*, 16(02), 1998, 207–218. https://doi.org/10.1017/S0263574798000538